The Direct Synthesis of H_2O_2 and Selective Oxidation of Methane to Methanol Using HZSM-5 Supported AuPd Catalysts

Richard J. Lewis[1] · Alejandro Bara-Estaun[1] · Nishtha Agarwal[1] · Simon J. Freakley[1,2] · David J. Morgan[1] · Graham J. Hutchings[1]

Abstract

In this study we show that using gold palladium nanoparticles supported on a commercial aluminosilicate (HZSM-5) prepared using a wet co-impregnation method it is possible to produce hydrogen peroxide from molecular H_2 and O_2 via the direct synthesis reaction. Furthermore, we investigate the efficacy of these catalysts towards the oxidation of methane to methanol using commercially available H_2O_2. The effect of SiO_2: Al_2O_3 ratio and calcination temperature is evaluated and a direct correlation between support acidity and the catalytic activity towards H_2O_2 synthesis and methanol production is observed.

Graphic Abstract
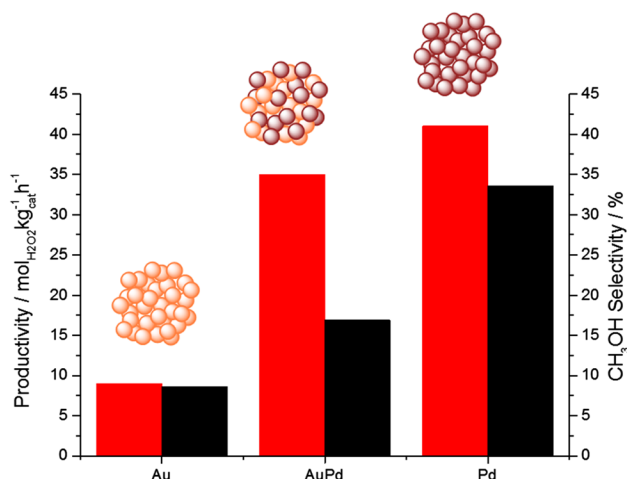
Electronic supplementary material The online version of this article (https://doi.org/10.1007/s10562-019-02876-7) contains supplementary material, which is available to authorized users.

✉ Graham J. Hutchings
  Hutch@cardiff.ac.uk

1 Cardiff Catalysis Institute, School of Chemistry, Cardiff University, Main Building, Park Place, Cardiff CF10 3AT, UK

2 Department of Chemistry, University of Bath, Claverton Down, Bath BA2 7AY, UK

1 Introduction

Hydrogen peroxide (H_2O_2) is a powerful oxidant with a high active oxygen content (47%) that offers significant benefits over other commonly used oxidants such as t-BuOOH, NaClO and permanganate which require costly separation and purification of waste by-products from product streams. In comparison the use of H_2O_2 as an oxidant produces H_2O only as a by-product, with an associated reduction in separation costs. Currently the majority of H_2O_2 produced is

utilised in the paper/pulp bleaching and textile industries as well as in the chemical synthesis sector, with the growing demand for H_2O_2 in recent years driven significantly by the increased production of propylene oxide [1] (via the integrated HPPO process) and cyclohexanone oxime (via cyclohexanone ammoximation) [2] which are key intermediates in the production of polyurethane and Nylon-6 respectively. Furthermore, H_2O_2 finds significant application in organo-sulphur oxidation [3], alkene epoxidation [4] and is finding increased use in the treatment of industrial waste streams, in part due to increasing desire to limit the use of chloride containing oxidants [5]. With the application of in situ generated H_2O_2 coupled with Fenton's reaction in the treatment of wastewater has widely reported [6–10].

Current global demand for H_2O_2 is expected to exceed 5.5 million tons per year by 2020 [11], with the vast majority (95%) of demand met via the anthraquinone oxidation (AO) process. Although highly efficient the AO process has several drawbacks, namely the requirement for the continual replacement of the anthraquinone molecule, which acts as the hydrogen carrier, and the high energy costs associated with the distillation, transport, storage and dilution of highly concentrated H_2O_2 solutions. With H_2O_2 often transported to the end user in concentrations in excess of 70 wt%, despite many on-site applications of H_2O_2 requiring concentrations of H_2O_2 of approximately 1–2 wt% [12]. The instability of H_2O_2 at relatively mild temperatures often requires the use of acidic stabilising agents to inhibit its decomposition to H_2O [13, 14]. The use of these stabilising agents can often lead to additional costs associated with reactor corrosion as well as the removal of impurities from product streams.

The direct synthesis of H_2O_2 from H_2 and O_2 provides an environmentally and economically attractive alternative to current means of H_2O_2 production on an industrial scale, by avoiding the need for the concentration, transportation, storage and dilution of H_2O_2 to desirable concentrations at point of use. The high catalytic activity of supported Pd catalysts towards H_2O_2 formation is well known [15–17], however low catalytic selectivity is often a concern and requires the use of halide and acid additives to inhibit the degradation of H_2O_2 via decomposition and hydrogenation pathways, which result in the formation of H_2O [18–20]. The low selectivity of mono-metallic Pd catalysts has been shown to be overcome through the addition of Au, with electronic, structural and isolation effects, or a combination of these factors all potential causes for the enhanced selectivity of AuPd catalysts in comparison to Pd analogues.

We [21–23] have previously reported the efficacy of AuPd nanoparticles supported on a range of zeolites, for the production of H_2O_2 as well as their use in the oxidation of cyclohexene and 2-butenol [24]. Further work has demonstrated the feasibility of in situ H_2O_2 generation in the hydroxylation of benzene [25, 26] and cyclohexane [27].

The oxidation of C_1–C_3 alkanes utilising H_2O_2 in conjunction with HZSM-5 [28–32] in addition to AuPd nanoparticles supported on TiO_2 [33, 34] at low temperature have been extensively reported, with the valorisation of methane to methanol in particular an attractive option to produce a versatile chemical feedstock. Indeed, we have previously reported that greater selectivity, at comparable catalytic productivity, towards methane can be achieved when generating H_2O_2 from H_2 and O_2 compared to preformed, commercially synthesised H_2O_2 [35]. Recently Agarwal et al. have shown that significant enhancement in catalytic activity can be achieved when utilising unsupported AuPd nanoparticles. The use of isotopically labelled $^{18}O_2$ demonstrated that in the presence of H_2O_2 that the resulting methanol incorporated a substantial fraction (70%) of gas-phase O_2 [36]. Further work by Petrov et al. has demonstrated the high activity of highly dispersed Pd within the mesoporous structure of dealuminated hierarchical mordenite. They report excellent catalytic performance with no deactivation over 90 h, in part due to through inhibiting Pd agglomeration through confinement within the zeolite structure [37].

Building on these previous works we now investigate the catalytic activity of AuPd nanoparticles supported on HZSM-5 for the direct synthesis of H_2O_2 from molecular H_2 and O_2 as well as for the selective oxidation of methane to methanol.

2 Experimental

2.1 Catalyst Preparation

Prior to co-impregnation of metal salts NH_4-ZSM-5 (Zeolyst) was calcined in flowing air (550 °C, 3 h, 20 °C min^{-1}) according to our previous work [38]. Mono- and bi-metallic Au–Pd/HZSM-5 catalysts have been prepared (on a weight metal basis) by wet co-impregnation of metal salts, based on methodology previously reported in the literature [39]. The procedure to produce 0.5%Au–0.5%Pd/H-ZSM-5 (1 g) is outlined below.

$PdCl_2$ (0.83 mL, 6 mg mL^{-1}, Sigma Aldrich) and $HAuCl_4\cdot3H_2O$ solution (0.41 mL, 12.25 mg mL^{-1}, Strem Chemicals) were charged into a 50 mL round bottom flask, with total volume adjusted to 16 mL with deionised water. The metal solution was heated to 65 °C in an thermostatically controlled oil bath with stirring, followed by the addition of HZSM-5 (0.95 g). The resulting mixture was then heated to 85 °C for 16 h. The resulting material was collected and ground prior to calcination in static air (400 °C, 3 h, 20 °C min^{-1}). The SiO_2: Al_2O_3 ratio is denoted in parentheses so that the 0.5%Au–0.5%Pd/HZSM-5(30) catalyst has a SiO_2: Al_2O_3 ratio of 30.

2.2 Direct Synthesis of H$_2$O$_2$

Hydrogen peroxide synthesis was evaluated using a Parr Instruments stainless steel autoclave with a nominal volume of 100 mL and a maximum working pressure of 14 MPa. To test each catalyst for H$_2$O$_2$ synthesis, the autoclave was charged with catalyst (0.01 g), solvent (5.6 g MeOH and 2.9 g H$_2$O). The charged autoclave was then purged three times with 5% H$_2$/CO$_2$ (0.7 MPa) before filling with 5% H$_2$/CO$_2$ to a pressure of 2.9 MPa, followed by the addition of 25% O$_2$/CO$_2$ (1.1 MPa). The temperature was held at 20 °C followed by stirring (1200 rpm) of the reaction mixture for 0.5 h. The above reaction parameters represent the optimum conditions we have previously used for the synthesis of H$_2$O$_2$. H$_2$O$_2$ productivity was determined by titrating aliquots of the final solution after reaction with acidified Ce(SO$_4$)$_2$ (0.01 M) in the presence of ferroin indicator. Catalyst productivities are reported as mol$_{H2O2}$ kg$_{cat}^{-1}$ h^{-1}.

2.3 Degradation of H$_2$O$_2$

Catalytic activity towards H$_2$O$_2$ was determined in a manner similar to the direct synthesis activity of a catalyst. The autoclave was charged with MeOH (5.6 g), H$_2$O$_2$ (50 wt% 0.69 g) HPLC standard H$_2$O (2.21 g) and catalyst (0.01 g), with the solvent composition equivalent to a 4 wt% H$_2$O$_2$ solution. From the solution 2 aliquots of 0.05 g were removed and titrated with acidified Ce(SO$_4$)$_2$ solution using ferroin as an indicator to determine an accurate concentration of H$_2$O$_2$ at the start of the reaction. The autoclave was pressurised with 2.9 MPa 5% H$_2$/CO$_2$ and the temperature was held at 20 °C and the reaction mixture was stirred at 1200 rpm for 0.5 h. After the reaction was complete the catalyst was removed from the reaction solvents and as previously two aliquots of 0.05 g were titrated against the acidified Ce(SO$_4$)$_2$ solution using ferroin as an indicator. The degradation activity is reported as mol$_{H2O2}$ h^{-1} kg$_{cat}^{-1}$.

2.4 Methane Oxidation Using Preformed H$_2$O$_2$

The oxidation of methane was carried out using a Parr stainless steel autoclave with a nominal volume of 50 mL reactor. Reactions were carried out using a 10 mL reaction mixture comprising an aqueous solution of H$_2$O$_2$ (10 mL, 0.1 M, 1000 μmol) and catalyst (0.027 g). Prior to use, the reactor was purged with methane (0.7 MPa) before being pressurized with methane to 3.05 MPa. The autoclave was then heated to the desired reaction temperature (50 °C), once at the set temperature, the reaction solution was stirred at 1500 rpm for 0.5 h. After the reaction was complete the stirring was stopped and the temperature was reduced to 10 °C using ice in order to minimize the loss of volatile products. Gaseous samples were analysed via gas chromatography (Varian-GC, equipped with a CPSIL5CB column [50 m, 0.33 mm internal diameter) fitted with a methanizer and flame ionization detector (FID)]. The reaction mixture was filtered to remove catalyst and analyzed by ^{1}H NMR, using a Bruker 500 MHz Ultrashield NMR spectrometer. All ^{1}H NMR samples were analyzed against a calibrated insert containing tetramethylsilane (TMS) in deuterated chloroform (99.9% D). The remaining H$_2$O$_2$ was determined by titration with acidified Ce(SO$_4$)$_2$.

2.5 Characterisation

Investigation of the bulk structure of the materials was carried out using powder X-ray diffraction (XRD) on a (θ–θ) PANalyticalX'pert Pro powder diffractometer using a Cu Kα radiation source operating at 40 keV and 40 mA. Standard analysis was performed using a 40 min scan between 2θ values of 10–80° with the samples supported on an amorphous silicon wafer. Diffraction patterns of phases were identified using the ICDD data base.

XPS measurements were carried out using a Kratos Axis UltraDLD spectrometer using monochromatic AlKα radiation (source power 120–180 W). An analyser pass energy of 160 eV was used for survey scans, and 40 eV for detailed acquisition of individual elemental regions. Samples were mounted using double-sided adhesive tape, and binding energies referenced to the C (1 s) binding energy of adventitious carbon contamination taken to be 284.7 eV. Spectra were quantified using CasaXPS and surface compositions (at.%) of the different samples.

Fourier-transform infrared spectroscopy (FTIR) was carried out with a Bruker Tensor 27 spectrometer fitted with a HgCdTe (MCT) detector and operated with OPUS software.

N$_2$ isotherms were collected on a Micromeritics 3Flex. Samples (ca. 0.020 g) were degassed (150 °C, 6 h) prior to analysis. Analyses were carried out at 77 K with P0 measured continuously. Free space was measured post-analysis with He. Pore size analysis was carried out using Micromeritics 3Flex software, N$_2$-cylindrical pores- oxide surface DFT model.

Temperature programmed desorption (TPD) of ammonia for HZSM-5 supported catalysts was carried out using a Quantachrome Industries ChemBET TPR/TPD chemisorption analyser, fitted with a thermal conductivity detector (TCD). The sample (0.05 g) was pre-treated for 1 h at 550 °C (15 °C min^{-1}) in He (145 mL min^{-1}). Ammonia was adsorbed at room temperature for 15 min to ensure saturation. Physisorbed ammonia was then removed at 100 °C (1 h, 15 °C min^{-1}) in He (80 mL min^{-1}). Chemisorbed ammonia was subsequently desorbed by heating to 900 °C (10 °C min^{-1}) in a flow of He (80 mL min^{-1}) with ammonia desorption monitored using a TCD with a current of 180 mV, and an attenuation of 1.

Metal leaching was quantified using microwave plasma atomic emission spectroscopy (MP-AES). Post-reaction solid catalysts were digested (0.01 g catalyst, 10 mL aqua-regia, 16 h) prior to analysis using an Agilent 4100 MP-AES.

3 Results and Discussion

Our initial studies compared the activity of mono- and bi-metallic Au–Pd/H-ZSM-5 (30) catalysts for the direct synthesis and subsequent degradation of H_2O_2 (Table 1). It was observed that the monometallic 1%Au/H-ZSM-5(30) catalyst has limited activity towards both H_2O_2 synthesis (9 mol_{H2O2} kg_{cat}^{-1} h^{-1}) and showed no activity towards the subsequent degradation of H_2O_2. In comparison the 1%Pd/HZSM-5(30) catalyst was seen to have much greater rates of H_2O_2 synthesis (41 mol_{H2O2} kg_{cat}^{-1} h^{-1}) and degradation (96 mol_{H2O2} kg_{cat}^{-1} h^{-1}). This is consistent with many pre-vious studies investigating AuPd nanoparticles supported on various oxide supports, with H_2O_2 degradation rates over mono-metallic Pd catalysts significantly higher than the analogous mono-metallic Au catalysts [40–42]. Indeed the rate of H_2O_2 production is greater than that previously reported for the analogous catalyst supported on TiO_2 (23 mol_{H2O2} kg_{cat}^{-1} h^{-1}) [43].

The addition of Au to supported Pd catalysts has been reported in the literature to enhance catalytic performance, through the inhibition of H_2O_2 degradation pathways. Although the means by which Au addition enhances cat-alytic performance is still unknown a range of potential causes have been suggested in the literature. Density func-tional theory (DFT) calculations have suggested that increasing numbers of neighbouring Au atoms around Pd can result in a decrease in electron back-donation into the π^* orbital of the O–O bond, which in turn inhibits the formation of H_2O through the cleavage of the O–O bond [44, 45]. Like-wise spectroscopic studies reveal that the addition of Au to Pd clusters is able to reduce the formation of H_2O through

isolation of contiguous Pd ensembles, known to favour the formation of H_2O compared to H_2O_2 [46, 47]. It is likely that a combination of both ensemble and isolation effects result in an enhancement in catalytic selectivity towards H_2O_2.

In keeping with previous studies investigating the co-impregnation of Au and Pd onto a range of oxide supports, the combination of both precious metals on HZSM-5(30) to produce bimetallic 0.5%Au–0.5%Pd/HZSM-5(30) results in an enhanced H_2O_2 synthesis activity (35 mol_{H2O2} kg_{cat}^{-1} h^{-1}), greater than that observed over a physical mixture of the mono-metallic catalysts with an analogous metal load-ing (12 mol_{H2O2} kg_{cat}^{-1} h^{-1}). However, the activity of the 0.5%Au–0.5%Pd/HZSM-5(30) catalyst does not supersede that of the 1%Pd/HZSM-5(30) catalyst, with the enhanced activity of bi-metallic AuPd nanoparticles previously observed to offer greater activity than the analogous Pd-only catalyst when utilising a range of oxide supports [48–50]. We attribute this to a lack of complete alloying and only par-tial formation of the Au-core PdO-shell typically adopted on oxide supports, indeed this is in keeping with our previous studies investigating the catalytic activity of AuPd catalysts supported on SiO_2 [51] and TS-1 [23]. It should be noted that catalytic activity of AuPd supported nanoparticles on HZSM-5(30) is significantly less active than that observed for the analogous catalyst supported on TiO_2, with this believed to be related to formation of the Au-core PdO-shell morphology adopted when utilising TiO_2 as a support. How-ever, the 0.5%Au–0.5%Pd/HZSM-5(30) catalyst displays far greater selectivity towards H_2O_2, with a H_2O_2 degradation rate (37 mol_{H2O2} kg_{cat}^{-1} h^{-1}) over three times lower than that observed for the analogous TiO_2 supported catalyst (130 mol_{H2O2} kg_{cat}^{-1} h^{-1}).

The activity of supported and colloidal AuPd nanoparti-cles for the selective oxidation of methane to methanol has been well studied [33, 35, 52], with the use of preformed H_2O_2 in conjunction with AuPd nanoparticles shown to aid in the activation of methane and the incorporation of a substantial fraction gas-phase O_2 (70%) [36]. Following

Table 1 Catalytic activity of mono- and bi-metallic 1% AuPd/HZSM-5 catalysts toward the direct synthesis and degradation of H_2O_2

Catalyst	Productivity (mol_{H2O2} kg_{cat}^{-1} h^{-1})[a]	Degradation (mol_{H2O2} kg_{cat}^{-1} h^{-1})[b]
1% Au/HZSM-5 (30)	9	0
1% Pd/HZSM-5 (30)	41	96
0.5% Au–0.5% Pd/HZSM-5 (30)	35	37
0.5% Au/HZSM-5 (30)+0.5% Pd/HZSM-5 (30)	12	23
HZSM-5 (30)	0	0
0.5% Au–0.5% Pd/TiO_2	90	130
TiO_2	0	0

[a]H_2O_2 direct synthesis reaction conditions: catalyst (0.01 g), H_2O (2.9 g), MeOH (5.6 g), 5% H_2/CO_2 (420 psi), 25% O_2/CO_2 (160 psi), 0.5 h, 20 °C 1200 rpm

[b]H_2O_2 degradation reaction conditions: catalyst (0.01 g), H_2O_2 (50 wt% 0.68 g) H_2O (2.22 g), MeOH (5.6 g), 5% H_2/CO_2 (420 psi), 0.5 h, 20 °C 1200 rpm

on from these previous studies we investigated the activity of HZSM-5(30) supported AuPd catalysts for methane oxidation, with our initial findings seen in Table 2. It can be seen that following high temperature calcination (550 °C) HZSM-5(30) displays significant catalytic activity for the selective oxidation of methane using aqueous conditions, at low temperature, when used in conjunction with preformed H_2O_2. The high activity of the HZSM-5 zeolite previously been reported by Hammond et al. who compared HZSM-5(30) to other zeolites with similar compositions, including TS-1 and zeolite-β [28]. Upon immobilisation of precious metals catalytic performance is greatly improved with both the 0.5%Au–0.5%Pd/HZSM-5(30) (16.9%) and 1%Pd/HZSM-5(30) (33.6%) catalysts offering higher selectivity towards methanol than the bare support, with the high catalytic performance of zeolite supported Pd catalysts for the complete oxidation of methane well known [53–55]. It is possible to correlate catalytic activity with total Pd content and we propose the presence of Pd is key for the selective transformation of methyl hydroperoxide (CH_3OOH) to methanol. By comparison the 1%Au/HZSM-5(30) catalyst is observed to offer the lowest selectivity to methanol (8.6%), comparable to that of HZSM-5(30) only, but does offer the greatest selectivity towards CH_3OOH, with CH_3OOH a key intermediate in the production of methanol [35]. It should be noted that the HZSM-5(30) supported catalysts greatly outperform the previously studied 0.5%Au–0.5%Pd/TiO₂ catalyst under similar reaction conditions, indeed the selectivity of the 1%Pd HZSM-5(30) catalyst is nearly 3 times that of the catalyst 0.5%Au–0.5%Pd/TiO₂ (12.1%).

Investigation of the calcined 0.5%Au–0.5%Pd/HZSM-5(30) catalyst by Fourier-transform infrared spectroscopy (FTIR) (Fig. S.1) reveals no discernible change in the observed positions of the absorption bands associated with HZSM-5 (30) upon calcination. Indeed, no discernible changes in the structure of HZSM-5 are observed even when exposed to calcination at 800 °C. It is possible to observe three distinct infrared bands in the FTIR spectra of 0.5%Au–0.5%Pd/HZSM-5 (30) at 800, 1060 and 1220 cm⁻¹ characteristic of SiO_4 tetrahedron units. The adsorption band around 1060 cm⁻¹ is attributed to the internal asymmetric stretching vibration of Si–O linkage and has been observed by Shirazi et al. to shift towards higher wavenumbers with increasing SiO_2: Al_2O_3 ratio of the zeolite [56]. While the adsorption band at 1220 cm⁻¹ has been utilised to provide information on the structure of ZSM-5 and have been assigned to the 5-membered rings present in the structure of the ZSM-5 zeolite and the band at 800 cm⁻¹ can be assigned the symmetric stretching of the external linkages of the SiO_4 tetrahedron.

Analysis by XRD (Fig. S.2, crystallite size shown in Table S.1) reveals that, as with FTIR analysis, there is no significant change in the MFI structure of HZSM-5 (30) upon metal impregnation and calcination when using the main reflection peaks associated with HZSM-5 (θ = 7.8, 8.8,14.8, 23.14, 23.91 and 24.5°) although our analysis does not take into account those reflections below 5°. The minor loss in MFI structure observed, as determined via crystallite size determination by XRD (Table S.1) is in keeping with work by Lu et al. who have previously reported no significant loss in crystallinity (6%) of HZSM-5 with calcination at similar temperatures to those investigated in this work and have further reported no change in surface area upon calcination of HZSM-5 as high as 800 °C [57]. Upon impregnation of the metals and calcination at 400 °C no reflections associated with either Au or Pd (either Pd^0 or Pd^{2+}) were observed. Indeed, even when these materials are exposed to calcination temperatures up to 800 °C no reflections associated with the precious metals are observed. The preservation of the MFI structure is believed to be key in maintaining the high catalytic performance of the HZSM-5 based catalysts for the selective oxidation of methane. With the high adsorption potential of the zeolitic structure crucial in producing an effective weakening of the C–H bond [58].

Table 2 The effect of calcination temperature on the catalytic activity of 0.5%Au–0.5%Pd/HZSM-5(30) catalyst toward the oxidation of methane using H_2O_2 added as co-reactant

Calcination temperature (°C)	Total products (µmol)	Product selectivity (µmol)				Oxy. Sel. (%)[a]	CH_3OH Sel (%)	H_2O_2 Con. (%)[b]
		CH_3OH	HCOOH	CH_3OOH	CO₂			
HZSM-5 (30)	3.15	0.29	0.84	1.89	0.13	96.0	9.3	25.0
1% Au/HZSM-5 (30)	5.45	0.47	2.81	2.04	0.13	97.6	8.6	17.6
1% Pd/HZSM-5 (30)	4.11	1.38	1.40	1.19	0.14	96.7	33.6	24.0
0.5% Au–0.5% Pd/HZSM-5 (30)	2.96	0.50	1.17	1.12	0.17	94.2	16.9	39.9
0.5% Au–0.5% Pd/TiO₂[c]	2.48	0.30	0	1.82	0.36	85.4	12.1	57.9

Methane oxidation reaction conditions: catalyst (0.027 g), H_2O (10 g), CH_4 (442 psi), 0.5 h, 50 °C, [H_2O_2] 0.1 M, 1500 rpm

[a]Oxygenate selectivity calculated as (moles oxygenates/total moles of products)×100

[b]Remaining H_2O_2 assayed by Ce^{4+}(aq) titration. H_2O_2 conversion calculated as ($mol_{initial}$/mol_{final})×100

[c]Conditions as stated but [H_2O_2] 0.5 M (result from ref [33])

Table 3 Summary of porosity and surface area of H-ZSM5 supported catalysts

Catalyst	Surface area[a] ($m^2 g^{-1}$)	$V_{Micropore}$ ($cm^3 g^{-1}$)
H-ZSM5 (30)[b]	495	0.183
0.5%Au–0.5%Pd/H-ZSM5 (30) (3 h, 400 °C, air)	453	0.170

[a]Surface area determined from nitrogen adsorption measurements using the BET equation

[b]ZSM-5 support exposed to calcination prior to metal immobilisation (flowing air, 550 °C, 3 h, 20 °C min^{-1})

The details of the textural properties of ZSM-5 (30) and the supported AuPd catalyst are summarised in Table 3 (Fig. S.3).

Immobilisation of metal nanoparticles on to the HZSM-5 (30) support is seen to decrease total surface area and total pore volume slightly from 495 $m^2 g^{-1}$ and 0.183 $cm^3 g^{-1}$ respectively for the bare HZSM-5 (30) support to 453 $m^2 g^{-1}$ and 0.170 $cm^3 g^{-1}$ respectively upon co-impregnation of the precious metals followed by calcination. We ascribe this decrease to result from the deposition of metal nanoparticles within the zeolitic pore structure. It should however be noted that despite this minimal loss in surface area and crystallinity, as determined by XRD, the introduction of precious metals have a significant effect on promoting the selective oxidation of methane.

Investigation into the effect of calcination temperature on the catalytic activity of the 0.5%Au–0.5%Pd/HZSM-5 (30) catalyst towards the direct synthesis of H_2O_2 and its subsequent degradation can be seen in Table 4. A direct correlation between calcination temperature and catalytic activity is observed, with increasing calcination temperature catalyst activity towards both H_2O_2 synthesis and degradation decreases, with catalytic activity towards H_2O_2 synthesis decreasing from 60 $mol_{H2O2} kg_{cat}^{-1} h^{-1}$ for the dried only catalyst to 35 $mol_{H2O2} kg_{cat}^{-1} h^{-1}$. Increasing calcination temperature beyond 400 °C leads to a further decrease in H_2O_2 production rate, which we ascribe to an increase in metal nanoparticle agglomeration, with Tian et al. elucidating the relationship between metal nanoparticle size and catalytic activity towards H_2O_2 formation [59].

Evaluation of catalyst activity upon re-use revealed that when calcined at 400 °C catalytic activity decreased to 35 $mol_{H2O2} kg_{cat}^{-1} h^{-1}$ but remained stable upon second use, which is in keeping with our previous studies into AuPd catalysts supported on TiO_2 [39] and TS-1 [23]. This loss in catalytic activity is attributed to leaching of active metals from the support with significant loss of both Au and Pd observed via MP-AES analysis for catalysts exposed to calcination temperatures below 400 °C. (Table S.2).

Further investigation into the effect of calcination temperature on the selective oxidation of methane can be seen in Table 5. It is observed that as calcination temperature increases there is a general trend of increasing methanol production, from 0.38 to 0.48 μmol as calcination temperature

Table 4 The effect of calcination temperature on the catalytic activity of 0.5%Au–0.5%Pd/HZSM-5 (30) towards H_2O_2 synthesis and its subsequent degradation

Calcination temperature (°C)	Productivity ($mol_{H2O2} kg_{cat}^{-1} h^{-1}$)[a]	Re-use productivity ($mol_{H2O2} kg_{cat}^{-1} h^{-1}$)[a]	H_2O_2 Degradation ($mol_{H2O2} kg_{cat}^{-1} h^{-1}$)[b]
200	54	29	43
400	35	35	37
800	18	18	10

[a]H_2O_2 direct synthesis reaction conditions: catalyst (0.01 g), H_2O (2.9 g), MeOH (5.6 g), 5% H_2/CO_2 (420 psi), 25% O_2/CO_2 (160 psi), 0.5 h, 20 °C 1200 rpm

[b]H_2O_2 degradation reaction conditions: catalyst (0.01 g), H_2O_2 (50 wt% 0.68 g) H_2O (2.22 g), MeOH (5.6 g), 5% H_2/CO_2 (420 psi), 0.5 h, 20 °C 1200 rpm

Table 5 The effect of calcination temperature on the catalytic activity of 0.5%Au–0.5%Pd/HZSM-5(30) catalyst toward the oxidation of methane using H_2O_2 as co-reactant

Calcination temperature (°C)	Total products (μmol)	Product selectivity (μmol)				Oxy. Sel. (%)[a]	CH_3OH Sel. (%)	H_2O_2 Con. (%)[b]
		CH_3OH	HCOOH	CH_3OOH	CO_2			
200	1.41	0.38	0.18	0.77	0.09	93.7	26.6	42.6
400	2.97	0.50	1.17	1.12	0.17	94.2	16.9	39.9
800	2.27	0.48	0.81	0.79	0.19	91.5	21.0	39.5

Methane oxidation reaction conditions: catalyst (0.027 g), H_2O (10 g), CH_4 (442 psi) 30.5 bar, 0.5 h, 50 °C, $[H_2O_2]$ 0.1 M, 1500 rpm

[a]Oxygenate selectivity calculated as (moles oxygenates/total moles of products)×100

[b]Remaining H_2O_2 assayed by Ce^{4+}(aq) titration. H_2O_2 conversion calculated as ($mol_{initial}/mol_{final}$)×100

rises from 200 to 800 °C. This is in keeping with Williams et al. [34] who have previously reported a dependence of methanol yield on calcination temperature for TiO_2 supported AuPd nanoparticles, with this enhancement ascribed to an increase in mean particle size. As with this previous study we report an enhancement in H_2O_2 utilisation with increasing calcination temperature the extent of H_2O_2 conversion decreases from 42.6 to 39.5%. We ascribe this to a combination of the improved H_2O_2 selectivity of larger AuPd nanoparticles [23, 60], known to form at higher calcination temperatures, and an increase in Pd: Au ratio, as determined by XPS (Table 6). With the latter indicating the possible enhancement of Au-core PdO-shell morphology known to be key in achieving high rates of H_2O_2 selectivity.

It has been previously reported that at calcination temperatures as low as 400 °C migration of Al from the zeolite framework can occur which has been correlated to result in a loss of Bronsted acidity [57]. Investigation of the effect of calcination temperature on the elemental composition of the surface of 0.5%Au–0.5%Pd/HZSM-5(30) as determined by XPS can be seen in Table 6, with the binding energies of Si 2p and Al 2p known to be characteristic of tetrahedral Si(IV) and Al(III) found in the MFI structure of HZSM-5 [61]. Upon impregnation of precious metals Si: Al ratio is seen to increase, indicating there is no observable Al migration, from 16.3 for the bare support to 21.1 for the sample calcined at 800 °C, this is believed to be a result of the preferential deposition of Au and Pd on external Al species. It should also be noted that a general increase in Pd: Au ratio is observed upon increasing calcination temperature with this ascribed to the enhancement of Pd surface segregation, well known to occur under an oxidative atmosphere.

Investigation into the effect of SiO_2: Al_2O_3 ratio on catalytic activity towards H_2O_2 synthesis and its subsequent degradation can be seen in Table 7, with Si: Al ratio confirmed by XPS (Table S.3). A negative correlation can be observed between Si content and H_2O_2 formation rate, with catalytic activity decreasing from 48 mol_{H2O2} kg_{cat}^{-1} h^{-1} for 0.5%Au–0.5%Pd/HZSM-5(23) to 6 mol_{H2O2} kg_{cat}^{-1} h^{-1} for

Table 7 The effect of varying the SiO_2:Al_2O_3 ratio of the HZSM-5 support on the activity of 0.5%Au–0.5%Pd/HZSM-5 catalysts toward the direct synthesis and degradation of H_2O_2

Support SiO_2 : Al_2O_3 ratio	Productivity (mol_{H2O2} kg_{cat}^{-1} h^{-1})[a]	Degradation (mol_{H2O2} kg_{cat}^{-1} h^{-1})[b]
23	48	27
30	35	37
80	19	74
280	6	162

[a]H_2O_2 direct synthesis reaction conditions: catalyst (0.01 g), H_2O (2.9 g), MeOH (5.6 g), 5% H_2/CO_2 (420 psi), 25% O_2/CO_2 (160 psi), 0.5 h, 20 °C 1200 rpm

[b]H_2O_2 degradation reaction conditions: catalyst (0.01 g), H_2O_2 (50 wt% 0.68 g) H_2O (2.22 g), MeOH (5.6 g), 5% H_2/CO_2 (420 psi), 0.5 h, 20 °C 1200 rpm

0.5%Au–0.5%Pd/HZSM-5(280), this also coincides with an increase in H_2O_2 degradation activity and is keeping with previous findings into the role of the support in determining catalytic selectivity [40, 62, 63].

As seen in Table 8 catalytic selectivity towards methanol can be related to Al_2O_3 content, with the 0.5%Au–0.5%Pd/HZSM-5(23) catalyst observed to offer the highest selectivity towards methanol (51.8%). As Al_2O_3 content decreases so too does catalytic selectivity towards methanol, with selectivity observed over the 0.5%Au–0.5%Pd/HZSM-5(280) (22.9%) catalyst less than half that of the analogous catalyst supported on HZSM-5(23), which is in keeping with previous work by Kalamaras et al. [64] The means by which a high Al_2O_3 content can enhance catalytic performance for the selective oxidation of methane is still of some debate. However, it is possible that the enhanced acidity of the support results in improved selectivity towards H_2O_2, with the enhanced stability of H_2O_2 over acidic supports well known [52]. Indeed the 0.5%Au–0.5%Pd/HZSM-5(280) catalyst is observed to convert far more H_2O_2 than the analogous catalysts supported on supports of greater proportion of Al_2O_3 and in turn higher acidity.

Table 6 Summary of the XPS derived surface atomic concentrations of 0.5% Au–0.5%Pd/HZSM-5 (30)

| Catalyst	Calcination temperature (°C)	Binding energy (eV)			Si : Al	Pd : Au
		Si 2p	Al 2p	O 1 s		
HZSM-5 (30)[a]	–	103.6	74.5	532.6	16.3	–
0.5%Au–0.5% Pd/ HZSM-5 (30)	Dried only	103.4	74.6	532.7	19.3	1.2
	200	103.4	74.6	532.7	18.5	3
	400	103.6	74.7	532.8	20.8	2
	800	103.9	75.2	533.1	21.1	4

[a]ZSM-5 support exposed to calcination prior to metal immobilisation (flowing air, 550 °C, 3 h, 20 °C min⁻¹)

Table 8 The effect of varying the SiO$_2$: Al$_2$O$_3$ ratio of the HZSM-5 support on the activity of 0.5%Au–0.5%Pd/HZSM-5 catalysts toward the oxidation of methane using H$_2$O$_2$ as co-reactant

Support SiO$_2$: Al$_2$O$_3$ ratio	Total products (μmol)	Product selectivity (μmol)				Oxy. Sel. (%)[a]	CH$_3$OH Sel. (%)	H$_2$O$_2$ Con. (%)[b]
		CH$_3$OH	HCOOH	CH$_3$OOH	CO$_2$			
23	1.38	0.71	0.12	0.12	0.42	69.3	51.8	51.8
30	2.97	0.50	1.17	1.12	0.17	94.2	16.9	39.9
80	0.96	0.3	0.2	0.5	0.1	92.8	27.2	32.8
280	2.5	0.6	0.9	1.0	0.1	94.8	22.9	62.7

Methane oxidation reaction conditions: catalyst (0.027 g), H$_2$O (10 g), CH$_4$ (442 psi), 0.5 h, 50 °C, [H$_2$O$_2$] 0.1 M, 1500 rpm

[a]Oxygenate selectivity calculated as (moles oxygenates/total moles of products)×100. [b] Remaining H$_2$O$_2$ assayed by Ce^{4+}(aq) titration. H$_2$O$_2$ conversion calculated as (mol$_{initial}$/mol$_{final}$)×100
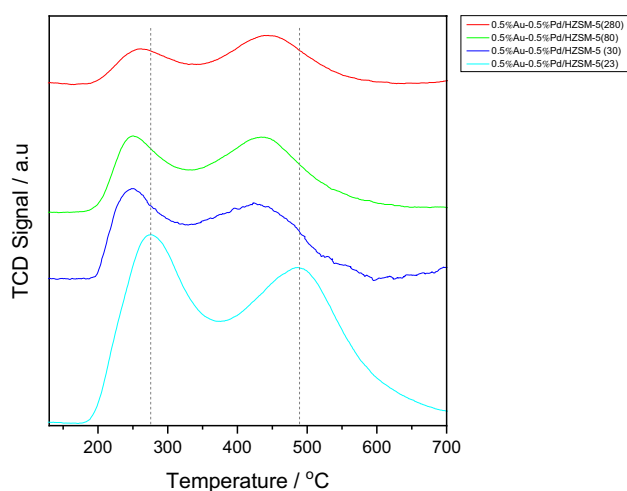
Fig. 1 NH$_3$-TPD profiles obtained for 0.5%Au–0.5%Pd/HZSM-5 as a function of SiO$_2$: Al$_2$O$_3$ ratio

To gain further insight into the role of SiO$_2$: Al$_2$O$_3$ on determining the acidity and in turn catalytic selectivity of the HZSM-5 supported catalysts NH$_3$-TPD analysis was carried out (Fig. 1).

Our analysis reveals two characteristic signals which can be associated with the MFI structure of ZSM-5 [65]. These desorption features are centred around 280 and 490 °C respectively with the low temperature peak attributed to adsorption at weak acid sites (Bronsted and Lewis) while the high temperature desorption is associated with strongly acidic Bronsted sites [66–68]. Bronsted acid sites are known to result from Al atoms connected to Si by a bridging hydroxyl, where the resultant negative charge is compensated for by a proton, while Lewis acid sites are composed of low coordination Al ions. It is therefore possible to relate overall acidity with Al content [56, 64, 69]. Our analysis by NH$_3$-TPD reveals that the proportion of strong acid sites increase with Al$_2$O$_3$ content, which we attribute to an increase in both framework and extra-framework Al content. In addition a shift in the desorption temperature associated with strong acid sites to lower temperatures is observed as Al content decreases, from 490 °C for 0.5%Au–0.5%Pd/HZSM-5(23) to 450 °C for 0.5%Au–0.5%Pd/HZSM-5(280), which has previously been reported and related to the presence of extra-framework Al [56]. It is well known that the acidity of the support can dramatically effect catalytic selectivity towards H$_2$O$_2$, with the choice of acidic supports influencing the degradation of H$_2$O$_2$ [40, 63, 70, 71]. It is therefore possible to correlate the enhanced selectivity towards H$_2$O$_2$ to the enhanced acidity of the support at lower SiO$_2$: Al$_2$O$_3$ molar ratios.

Further analysis by FTIR (Fig. S.4) reveals a shift in the asymmetric stretching frequencies at 1220 and 1040 cm^{-1} to higher wavenumbers with an increase in SiO$_2$: Al$_2$O$_3$ ratio and this can be correlated with the lower mass of Al compared to Si [72]. Al-Dughaither et al. have previously investigated the effect of increasing Al incorporation on relative crystallinity of HZSM-5, with only a minor increase in unit cell volume with increasing Al content, correlating with no significant effect on crystallinity [65]. Our own investigation via XRD (Figure S.5) is in keeping with this previous study, with no significant change within the MFI structure observed with increasing SiO$_2$: Al$_2$O$_3$ ratio.

4 Conclusion

In conclusion we have demonstrated that it is possible to generate H$_2$O$_2$ over AuPd supported HZSM-5 catalysts from molecular H$_2$ and O$_2$, at ambient temperature, with H$_2$O$_2$ synthesis activity seen to correlate with total Pd content. Furthermore, we have shown that through modification of the SiO$_2$: Al$_2$O$_3$ ratio and in turn the acidic strength of the support catalytic activity and selectivity towards H$_2$O$_2$ can be controlled. As with H$_2$O$_2$ synthesis catalytic performance towards the selective oxidation of methane to methanol has been investigated and is found to be related to both total Pd content as well as the acidity of the support, with catalytic activity of the HZSM-5 supported catalysts far superior to

the analogous catalysts supported on an oxide support. We believe that the activity of these catalysts to both the direct synthesis of H$_2$O$_2$ and the selective oxidation of methane to methanol make them an attractive avenue of study for the selective oxidation of methane to methanol via the in situ production of H$_2$O$_2$, avoiding the economic and environmental drawbacks associated with the use of preformed H$_2$O$_2$.

References

1. Lin M, Xia C, Zhu B, Li H, Shu X (2016) Chem Eng J 295:370–375
2. Liu G, Wu J, Luo H (2012) Chin J Chem Eng 20:889–894
3. Kaczorowska K, Kolarska Z, Mitka K, Kowalski P (2005) Tetrahedron 61:8315–8327
4. Peng C, Lu XH, Ma XT, Shen Y, Wei CC, He J, Zhou D, Xia QH (2016) J Mol Catal A: Chem 423:393–399
5. dwrcymru.com. (2019). Our water challenges. https://www.dwrcymru.com/en/Innovation/Our-Challenges/Our-Water-Challenges.aspx. Accessed 4 June 2019
6. Triki M, Contreras S, Medina F (2014) J Sol-Gel Sci Technol 71:96–101
7. Liu Y, Yu Z, Hou Y, Peng Z, Wang L, Gong Z, Zhu J, Su D (2016) Catal Commun 86:63–66
8. Yalfani MS, Contreras S, Medina F, Sueiras JE (2011) J Hazard Mater 192:340–346
9. Yalfani MS, Contreras S, Medina F, Sueiras J (2009) Appl Catal B 89:519–526
10. Underhill R, Lewis RJ, Freakley SJ, Douthwaite M, Miedziak PJ, Edwards JK, Akdim O, Hutchings GJ (2018) *Johnson Matthey*. Technol. Rev. 62:417–425
11. Seo M, Kim HJ, Han SS, Lee K (2017) Catal Surv Asia 21:1–12
12. Bianchi ML, Crisol R, Schuchardt U (1999) Bioresour Technol 68:17–21
13. Scoville JR, Novicova IA (1996) Cottrell Ltd., US5900256
14. Wegner P, Wegner Paul C (2003) US20050065052 A1
15. Arrigo R, Schuster ME, Abate S, Giorgianni G, Centi G, Perathoner S, Wrabetz S, Pfeifer V, Antonietti M, Schlögl R (2016) ACS Catal 6:6959–6966
16. Abate S, Arrigo R, Schuster ME, Perathoner S, Centi G, Villa A, Su D, Schlögl R (2010) Catal Today 157:280–285
17. Hu B, Deng W, Li R, Zhang Q, Wang Y, Delplanque-Janssens F, Paul D, Desmedt F, Miquel P (2014) J Catal 319:15–26
18. Ntainjua EN, Piccinini M, Pritchard JC, He Q, Edwards JK, Carley AF, Moulijn JA, Kiely CJ, Hutchings GJ (2009) ChemCatChem 1:479–484
19. Samanta C, Choudhary VR (2007) Catal Commun 8:2222–2228
20. Choudhary VR, Samanta C, Jana P (2007) Appl Catal A 317:234–243
21. Li G, Edwards JK, Carley AF, Hutchings GJ (2007) Catal Today 122:361–364
22. Li G, Edwards JK, Carley AF, Hutchings GJ (2006) Catal Today 114:369–371
23. Lewis RJ, Ueura K, Fukuta Y, Freakley SJ, Kang L, Wang R, He Q, Edwards JK, Morgan DJ, Yamamoto Y, Hutchings GJ (2019) ChemCatChem 11:1673–1680
24. Li G, Edwards JK, Carley AF, Hutchings GJ (2007) Catal Commun 8:247–250
25. Remias JE, Pavlosky TA, Sen A (2003) J Mol Catal A: Chem 203:179–192
26. Miyake T, Hamada M, Niwa H, Nishizuka M, Oguri M (2002) J Mol Catal A: Chem 178:199–204
27. Kuznetsova LI, Kuznetsova NI, Koscheeva OS (2017) Catal Commun 88:50–52
28. Hammond C, Forde MM, Ab Rahim MH, Thetford A, He Q, Jenkins RJ, Dimitratos N, Lopez-Sanchez JA, Dummer NF, Murphy DM, Carley AF, Taylor SH, Willock DJ, Stangland EE, Kang J, Hagen H, Kiley CJ, Hutchings GJ (2012) Angew Chem Int Ed 51:5129–5133
29. Armstrong RD, Peneau V, Ritterskamp N, Kiley CJ, Taylor SH, Hutchings GJ (2018) ChemPhysChem 19:469–478
30. Al-Shihri S, Richard CJ, Chadwick D (2017) ChemCatChem 9:1276–1283
31. Hammond C, Jenkins RJ, Dimitratos N, Lopez-Sanchez JA, Ab Rahim MH, Forde MM, Thetford A, Murphy DM, Hagen H, Stangland EE, Moulijn JM, Taylor SH, Willock DJ, Hutchings GJ (2012) Chem Eur J 18:15735–15745
32. Al-Shihri S, Richard CJ, Al-Megren H, Chadwick D (2018) Catal Today. https://doi.org/10.1016/j.cattod.2018.03.031
33. Ab Rahim MH, Armstrong RD, Hammond C, Dimitratos N, Freakley SJ, Forde MM, Morgan DJ, Lalev G, Jenkins RL, Lopez-Sanchez JA, Taylor SH, Hutchings GJ (2016) Catal Sci Technol 6:3410–3418
34. Williams C, Carter JH, Dummer NF, Chow YK, Morgan DJ, Yacob S, Serna P, Willock DJ, Meyer RJ, Taylor SH, Hutchings GJ (2018) ACS Catal 8:2567–2576
35. Ab Rahim MH, Forde MM, Jenkins RL, Hammond C, He Q, Dimitratos N, Lopez-Sanchez JA, Carley AF, Taylor SH, Willock DJ, Murphy DM, Kiely CJ, Hutchings GJ (2013) Angew Chem Int Ed 52:1280–1284
36. Agarwal N, Freakley SJ, McVicker RU, Althahban SM, Dimitratos N, He Q, Morgan DJ, Jenkins RL, Willock DJ, Taylor SJ, Kiely CJ, Hutchings GJ (2017) Science 358:223–227
37. Petrov AW, Ferri D, Krumeich F, Nachtegaal M, van Bokhoven JA, Kröcher O (2018) Nat Commun 9:2545
38. Xu J, Armstrong RD, Shaw G, Dummer NF, Freakley SJ, Taylor SH, Hutchings GJ (2016) Catal Today 270:93–100
39. Edwards JK, Solsona BE, Landon P, Carley AF, Herzing AA, Kiely CJ, Hutchings GJ (2005) J Catal 236:69–79
40. Ntainjua EN, Edwards JK, Carley AF, Lopez-Sanchez JA, Moulijn JA, Herzing AA, Kiely CJ, Hutchings GJ (2008) Green Chem 10:1162
41. Edwards JK, Solsona BE, Landon P, Carley AF, Herzing AA, Watanabe M, Kiely CJ, Hutchings GJ (2005) J Mater Chem 15:4595
42. Solsona BE, Edwards JK, Landon P, Carley AF, Herzing AA, Kiely CJ, Hutchings GJ (2006) Chem Mater 18:2689–2695
43. Sankar M, He Q, Morad M, Pritchard J, Freakley SJ, Edwards JK, Taylor SH, Morgan DJ, Carley AF, Knight DW, Kiely CJ, Hutchings GJ (2012) ACS Nano 6:6600–6613
44. Wilson NM, Flaherty DW (2016) J Am Chem Soc 138:574–586
45. Ham HC, Stephens JA, Hwang GS, Han J, Nam SW, Lim TH (2011) Catal Today 165:138–144

46. Jirkovský JS, Panas I, Ahlberg E, Halasa M, Romani S, Schiffrin DJ (2011) J Am Chem Soc 133:19432–19441
47. Plauck A, Stangland EE, Dumesic JA, Mavrikakis M (2016) Proc Natl Acad Sci USA 113:E1973–E1982
48. Herzing AA, Carley AF, Edwards JK, Hutchings GJ, Kiely CJ (2008) Chem Mater 20:1492–1501
49. Menegazzo F, Burti P, Signoretto M, Manzoli M, Vankova S, Boccuzzi F, Pinna F, Strukul G (2008) J Catal 257:369–381
50. Enache DI, Edwards JK, Landon P, Solsona BE, Carley AF, Herzing AA, Watanabe M, Kiely CJ, Knight DW, Hutchings GJ (2006) Science 311:362–365
51. Edwards JK, Parker SF, Pritchard J, Piccinini M, Freakley SJ, He Q, Carley AF, Kiely CJ, Hutchings GJ (2013) Catal Sci Technol 3:812
52. Ab Rahim MH, Forde MM, Hammond C, Jenkins RL, Dimitratos N, Lopez-Sanchez JA, Carley AF, Taylor SH, Willock DJ, Hutchings GJ (2013) Top Catal 56:1843–1857
53. Gélin P, Primet M (2002) Appl Catal B 39:1–37
54. Li Y, Armor JN (1994) Appl Catal B 3:275–282
55. de Correa CM, Aï´da Luz Villa H (1996) Appl Catal B 10:313–323
56. Shirazi L, Jamshidi E, Ghasemi MR (2008) Cryst Res Technol 43:1300–1306
57. Zhao Z, Lu J, Xu C, Duan A, Zhang P (2005) J Nat Gas Chem 14:213–220
58. Sastre G, Corma A (2009) J Mol Catal A 305:3–7
59. Tian P, Ouyang L, Xu X, Ao C, Xu X, Si R, Shen X, Lin M, Xu J, Han Y (2017) J Catal 349:30–40
60. Tian P, Ding D, Sun Y, Xuan F, Xu X, Xu J, Han Y (2019) J Catal 369:95–104
61. Moreno-Recio M, Santamaría-González J, Maireles-Torres P (2016) Chem Eng J 303:22–30
62. Lewis RJ, Edwards JK, Freakley SJ, Hutchings GJ (2017) Ind Eng Chem Res 56:13287–13293
63. Freakley SJ, Lewis RJ, Morgan DJ, Edwards JK, Hutchings GJ (2015) Catal Today 248:10–17
64. Kalamaras C, Palomas D, Bos R, Horton A, Crimmin M, Hellgardt K (2016) Catal Lett 146:483–492
65. Al-Dughaither AS, de Lasa H (2014) Ind Eng Chem Res 53:15303–15316
66. Ding C, Wang X, Guo X, Zhang S (2008) Catal Commun 9:487–493
67. Iwasaki M, Yamazaki K, Banno K, Shinjoh H (2008) J Catal 260:205–216
68. Dou B, Lv G, Wang C, Hao Q, Hui K (2015) Chem Eng J 270:549–556
69. Costa C, Dzikh IP, Lopes JM, Lemos F, Ribeiro FR (2000) J Mol Catal A 154:193–201
70. Blanco-Brieva G, Cano-Serrano E, Campos-Martin JM, Fierro JLG (2004) Chem Commun 0:1184–1185
71. Blanco-Brieva G, Montiel-Argaiz M, Desmedt F, Miquel P, Campos-Martin JM, Fierro JLG (2017) Top Catal 60:1151–1155
72. Ali MA, Brisdon B, Thomas WJ (2003) Appl Catal A 252:149–162